12-2018

Quasi-Particle Band Structure and Excitonic Effects in One-Dimensional Atomic Chains

Eesha Sanjay Andharia
University of Arkansas, Fayetteville

Quasi-Particle Band Structure and Excitonic Effects in One-Dimensional Atomic Chains

A thesis submitted in partial fulfillment
of the requirements for the degree of
Master of Science in Microelectronics-Photonics

by

Eesha Sanjay Andharia
SRM University
Bachelor of Technology in Nanotechnology, 2014

December 2018
University of Arkansas

This thesis is approved for recommendation to the Graduate Council.

Salvador Barraza-Lopez, Ph.D.
Thesis Director

Morgan E Ware, Ph.D.
Committee Member

Huaxing Fu, Ph.D.
Committee Member

Rick Wise, Ph.D.
Ex-Officio Member

The following signatories attest that all software used in this thesis were legally licensed for use by Eesha Sanjay Andharia for research purposes and publication.

Ms. Eesha Sanjay Andharia	Dr. Salvador Barraza Lopez, Thesis Director

This thesis was submitted to http://www.turnitin.com for plagiarism review by the TurnItIn company's software. The signatories have examined the report on this thesis that was returned by TurnItIn and attest that, in their opinion, the items highlighted by the software are incidental to common usage and are not plagiarized material.

Dr. Rick Wise, Program Director	Dr. Salvador Barraza Lopez, Thesis Director

Abstract

The high exciton binding energy in one dimensional (1D) nano-structures makes them prominent for optoelectronic device applications, making it relevant to theoretically investigate their electronic and optical properties. Many-body effects that are not captured by the conventional density functional theory (DFT) have a huge impact in such selenium and tellurium single helical atomic chains. This work goes one step beyond DFT to include the electron self-energy effects within the GW approximation to obtain a corrected quasi-particle electronic structure. Further, the Bethe-Salpeter equation was solved to obtain the absorption spectrum and to capture excitonic effects. Results were obtained using the Hyberstein-Louie (HL), and the Golby Needs (GN) generalized plasmon pole (GPP) models. The first bound excitonic state is well localized within 50 A along the c-axis of the crystal, with a high exciton binding energy of 2.5 eV (GN) and 2.78 eV (HL) for Se and 2.09 eV for (GN) and 2.28 eV (HL) for Te nano-wire.

Acknowledgements

First of all, I would like to thank my research advisor Dr. Salvador Barraza Lopez for giving me an opportunity to undertake the project pertaining to investigation of excitonic effects in nanostructures. His timely guidance and motivation helped me complete such a behemoth task. I would also like to thank my research group members, especially, post-doctoral fellow, Dr. Thaneshwor Prasad Kaloni for his technical guidance and support. I would also like to thank my course advisor and Micro-EP program Director, Dr. Rick Wise, for his persistent support and advice every now and then. I would also like to thank Micro-EP program specialist Ms. Renee Jones Hearon for support and friendly help & advice.

I would also take this opportunity to thank the National Energy Research Scientific Computing Center (NERSC) 'help and support' for their constant help and advice pertaining to technical issues while running simulations at Cori and Edison supercomputers. Pertaining to difficulties with the code, I thank Berkeley GW team for help and especially to its support forum, for constant emailing and responses.

Financial support was provided by the National Science Foundation (NSF), grant No. 1610126, and computational resources at NERSC under a grant from the Department of Energy (DOE). Any opinions, findings, and conclusions or recommendations expressed in this material are those of the author and do not necessarily reflect the views of the National Science Foundation.

Dedication

This thesis is dedicated to my parents and teachers.

Table of Contents

List of Figures

Chapter 1: Introduction

As shown in Figure 1.1, signal processing uses electrons in transistors whereas signal communication relies on photons in waveguides & optical fibers. An exciton – a bound electron-hole pair – with a bound energy larger than room temperature makes room temperature operation of excitonic devices possible [1,2], proffering further advantages such as high switching speed & signal to noise ratio, more compact & miniaturized devices [3], and fabrication of mixed dimensional van der Waal's (vdW's) hetero-structures [4].

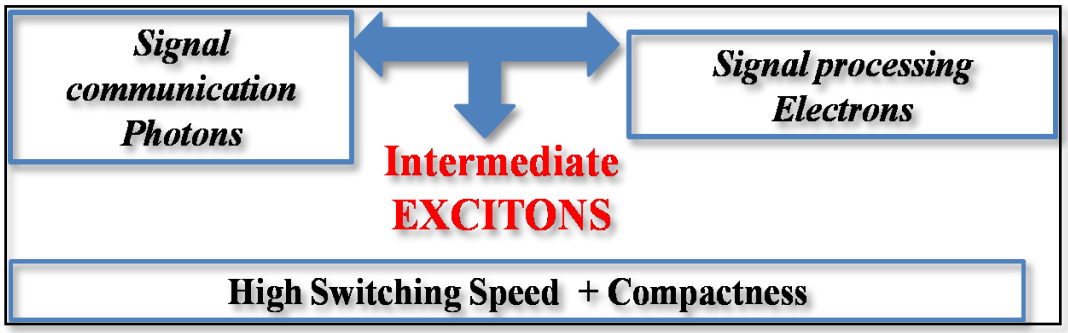

Figure 1.1 Application of excitonic devices.

As compared to conventional excitonic devices based on group II/1V and III/V compound (AlGaAs/GaAs) quantum wells (QW's) [5,6], a pristine class of van der Waal's based 2-dimensional [7,8] and 1-dimensional materials [9,10] have higher exciton binding energy due to quantum confinement and reduced dielectric screening. A high effective mass also leads to a large exciton binding energy of these materials.

Several 1D nanowires of silicon [11,12], carbon nanotubes [13], polymeric chains [14,15], boron nitride nanotubes [16], Ge [17] and Se & Te [18] nanowires exhibit a high exciton binding energy. This is an upshot of the electronic density of states (DOS) in one spatial dimension. Such a dependence of electronic properties has three critical effects: 1) widening of

the electronic bandgap, 2) changing its intrinsic band gap to direct, as compared to the indirect band gap in the bulk and 3) several inter-band or intra-band transitions of electrons. This necessitates the theoretical prediction of electronic and optical properties of such 1D vdW's based nanowires.

As shown in Figure 1.2, in its bulk crystalline form, Se and Te have a trigonal structure with 3 atoms forming helical chains weakly bonded via van der Waal's interaction. Thus, proffering the possibility of exfoliating single atomic chains. A tight-binding model of Se chains was reported by Olencha and Knox [19]. A DFT based study of the effect of confinement and diameter dependent electronic properties for Se and Te was undertaken by Waghmare et.al [20,21]. First principles calculation using density functional theory for determining electronic structure of solids does not capture the prominent many-body effects in such vdW's based Se and Te nano-wires and severely underestimates the band gap. A single-shot G_0W_0 calculation using the VASP [22] DFT code was limited by the xy-planar distance of only 10 Å [23]. This work goes one step beyond DFT to include electron self-energy corrections within the GW Approximation. Using the energy eigenvalues obtained from GW calculations, the Bathe-Salpeter equation is employed to calculate both, interacting and non-interacting absorption spectrum and excitonic states.

In Chapter 2, a comprehensive understanding of the formalism including the fundamentals of DFT, a self-consistent GW calculation and kernel of Bethe-Salpeter equation is given. All the pragmatic computation is based on this. Computational details including the type of vdW's interaction, pseudopotential, and generalized plasmon pole models are explained in Chapter 3. Followed by which, electronic (Chapter 4) and optical properties (Chapter 5) (including excitonic effects and its dominance on the absorption spectrum), in comparison to

bulk Se and Te nano-wires, is studied in detail and a spatial distribution of excitonic wave function for Se in real space is given. In a nutshell, the electronic and optical properties of Se and Te single helical chains have been investigated profoundly using ab-initio method.

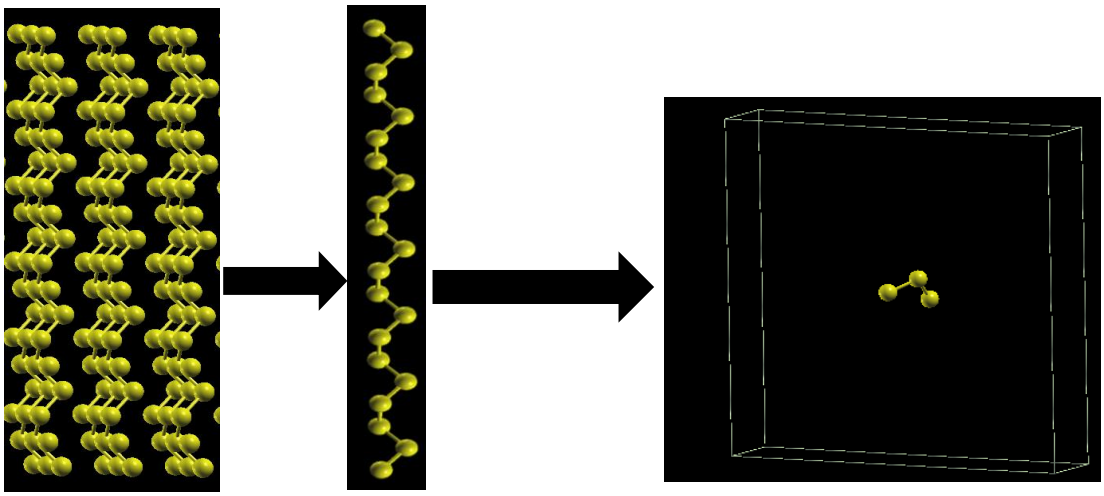

Figure 1.2 Crystal structure of Selenium and Tellurium single helical chains.

Chapter 2: Basic Formalism

The many-body Hamiltonian for a system of interacting electrons and nuclei is written as follows:

$$\widehat{H} = \frac{-\hbar^2}{2m_e}\sum_i \nabla_i^2 + \frac{-\hbar^2}{2M}\sum_I \nabla_I^2 + \sum_{i,I}\frac{Z_I e^2}{|r_i - R_I|} + \frac{1}{2}\sum_{i,j}\frac{e^2}{|r_i - r_j|} + \frac{1}{2}\sum_{I,J}\frac{Z_I Z_J e^2}{|R_I - R_J|}$$

(Equation 2.1)

Wherein, i & j runs over all the electrons in the system, I & J indices describe all the nuclei, m_e is the mass of an electron and M is the mass of nuclei. The first and second terms are the kinetic energy of electrons and nuclei, respectively. The third term represents the Coulomb interaction between electrons and nuclei, followed by the electron-electron interaction in the fourth term. Finally, the last term represents the classical Coulomb interaction among nuclei.

In what follows, nuclei terms are neglected so that the interacting many body Hamiltonian can be written as follows:

$$\widehat{H} = \hat{T} + \widehat{V_{int}} + \widehat{V_{ext}} + E_{II} \qquad \text{(Equation 2.2)}$$

Where, $\hat{T}$ is the kinetic energy operator, $\widehat{V_{ext}}$ is potential on electrons due to nuclei, E_{II} is classical interaction of nuclei with each other and $\widehat{V_{int}}$ is electron-electron self-interaction. The total energy of the system is expectation value of the above Hamiltonian:

$$E = < T > + < V_{int} > + \int d^3 r V_{ext} n(r) + E_{II} \qquad \text{(Equation 2.3)}$$

Here, $n(r)$ is electron density at a given spatial coordinate r.

At this point it is important to define all the classical coulombian energies, E^{CC},

$$E^{CC} = E_{Hartree} + \int d^3 r V_{ext} n(r) + E_{II} \qquad \text{(Equation 2.4)}$$

where the Hartree energy, $E_{Hartree}$ is self- interaction electron density treated as classical charge density. Now, the total energy expression is as follows:

$$E = < T > + < V_{int} - E_{Hartree} > + E^{CC} \qquad \text{(Equation 2.5)}$$

The difference between the interacting, correlated electron density, V_{int}, and the classically interacting charge density, $E_{Hartree}$ is defined as the exchange correlation energy, E_{XC}.

There are two independent electron approximations: Hartree and Hartree-Fock; electrons obey Pauli's exclusion principle in the Hartree-Fock approximation by construction. The Hartree approximation, on the other hand, assumes that the electronic wave functions are a product of independent particle orbitals whereas Hartree-Fock imposes an anti-symmetry on the many-body wave function, giving a Slater determinant of independent electron orbitals at a point r with spin σ:

$$V_H(r) = \sum_n \frac{e^2|\varphi_n(r')*\varphi_n(r)|}{|r - r'|} \qquad \text{(Equation 2.6)}$$

and

$$V_{HF} = V_H(r) + V_{ex} \qquad \text{(Equation 2.7)}$$

However, the true many-body wave function is a product of many such Slater determinants, in the so-called configuration interaction. The difference between the exact and the HF solution is defined as the correlation energy.

For a system with N electrons, such an approach leads to 3N differential equations. Suppose a system has 50 electrons. The spatial part of many electronic wave function will have 3N, i.e., 150 spatial degrees of freedom. Further, if the K-grid has 50 K-points, there are a total 50^{150} calculations to be performed which makes it pragmatically impossible to solve computationally. Thus, one cannot use single electron orbitals as a basic quantity. A different

quantity is used that does not directly depend on the number of electrons: such quantity is the electron density, which depends only on spin and three spatial coordinates.

2.1 Density Functional Theory (DFT)

As the name suggests, in principle all the properties of interacting many body systems can be expressed as functional of the electron density. The electron density operator can be written as:

$$\hat{\rho} = \sum_i |\Psi_i > f_i < \Psi_i| \qquad \text{(Equation 2.8)}$$

where, f_i is Fermi-Dirac distribution function which gives the probability of finding an electron in state i as per Equation 2.9.

$$f_i = \frac{1}{e^{\beta(E_i - E_f)} + 1} \qquad \text{(Equation 2.9)}$$

where, E_f is the Fermi energy. More explicitly, for spin σ and position r, density can be written as diagonal part of the matrix:

$$\rho(r, \sigma, r', \sigma') = \delta_{\sigma\sigma'} \sum_i \Psi_i^{\sigma *} f_i \Psi_i^{\sigma} \qquad \text{(Equation 2.10)}$$

Hohenberg and Kohn formulated two fundamental theorems. The first one sets up a direct link between the external potential V_{ext} and, hence, the many body Hamiltonian given in Equation 2.2 and the true ground state density of interacting electronic system, i.e., external potential uniquely determines the electronic density of the system, except for a constant [24]. The second theorem states that a minimum in the energy functional corresponds to true ground state electronic density.

The density dependent energy functional can be written as follows:

$$E_V[\rho] = T_S[\rho] + \int V_{ext}(r)\rho(r)dr + \frac{1}{2}\int \frac{\rho(r)\rho(r')}{|r - r'|} dr dr' + E_{XC}[\rho] \qquad \text{(Equation 2.11)}$$

The correlation term in DFT includes the effect of interacting kinetic energy contributions with equivalent electron density. If an exact form of the energy functional was found, one could easily obtain the ground state energy of the system by minimizing the functional with respect to the electron density.

However, an exact form of exchange-correlation functional, E_{XC} is not known. In general, one uses Kohn-Sham ansatz [25], which states that for a given external potential of a truly interacting system, there exists an auxiliary system with the same electron density as the real system. The Kohn Sham equations are solved self consistently to obtain the eigenvalues and eigenfunctions as shown in Figure 2.1 below:

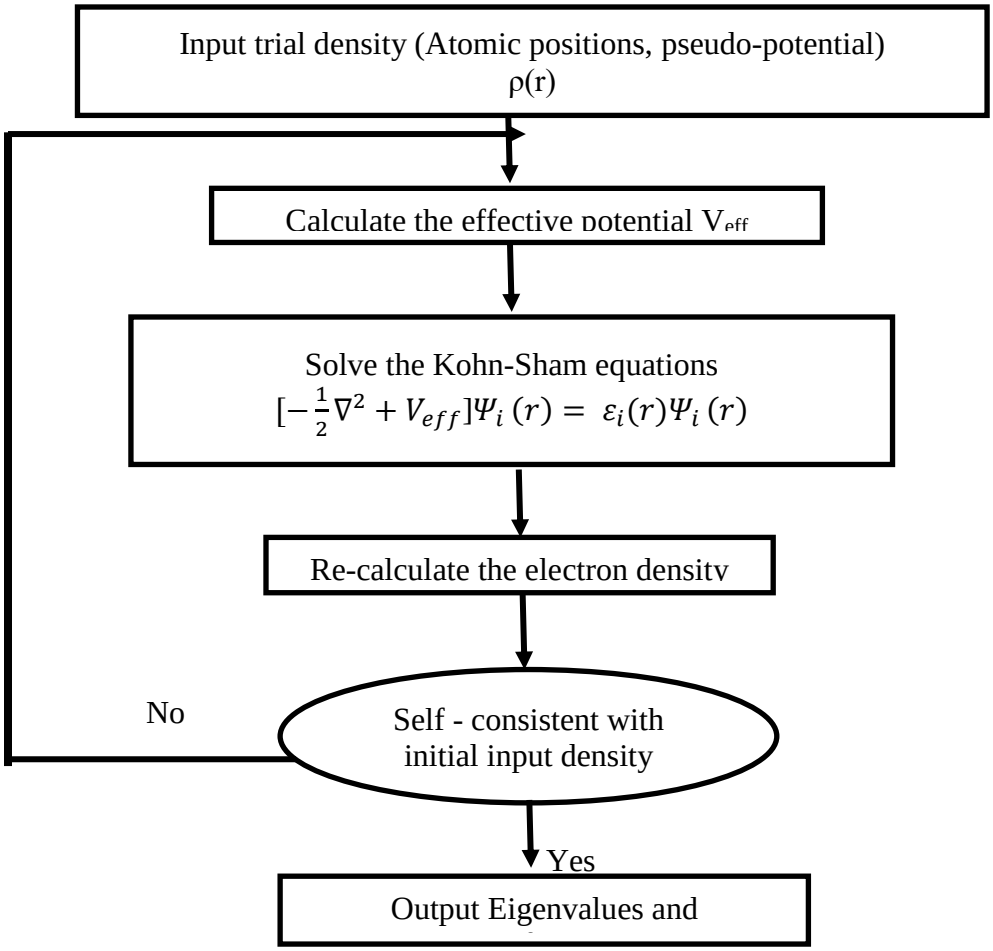

Figure 2.1 Self-consistent Kohn-Sham cycle.

In a self-consistent calculation, the initial density is used to calculate an effective potential, known as the Kohn-Sham (KS) potential, which is used to solve the KS equations to obtain KS eigenvalues and eigenfunctions. These, in turn, are used to calculate new electron density. If not converged within a given precession, the cycle is iterated with the previous output density as new input density.

In practice, one must assume that the exchange correlation energy is a function of a non-varying electron density in space. This is known as local density approximation and is formulated as:

$$E_{xc}[n] = \int \rho(r) e_{xc}(r) d^3r \qquad \text{(Equation 2.12)}$$

However, any real electronic system will be non-homogeneous, i.e., it has a varying electron density in space. As a better approximation, one expands the exchange correlation functional in terms of gradients of the electron density, $\nabla n(r)$. This is known as the generalized gradient approximation (GGA) and is added with higher order derivatives to the LDA values.

Although qualitatively correct, Kohn-Sham eigenvalues are quantitatively wrong. One cannot interpret the Kohn-Sham values as exact excitation energies of single particle states, except the value of highest occupied state which corresponds to the ionization energy or chemical potential of metals. The value of bandgap is underestimated by as much as 1 eV. Hence, one relies on the many body perturbation theory that considers electron self-energy effects to obtain a more accurate electronic structure.

2.2 GW Approximation for Self-Energy Corrections

Experimentally, the electronic band gap is determined via photoelectron spectroscopic techniques. In the direct photoelectron method, a photon ejects an electron with some kinetic energy and the difference between the photon energy and the electron kinetic energy yields the

binding energy of the electron and hence an estimate of the band gap. In reality, the electrons are correlated with each other via electrostatic Coulomb interaction, and such an ejection or emission is a many body process.

In such a process, the repulsive Coulomb interaction amongst the electrons will create a positively charged hole surrounding the electron. Such an ensemble of negatively charged electrons surrounded by positively charged holes behaves as an individual particle and is defined as a quasi-particle that sees a reduced Coulomb interaction. Such an effect is determined by a variable called the screened Coulomb interaction, W.

To account for such quasi-particle properties, we rely on electron self-energy effects. The many-body Hamiltonian can be written as follows:

$$\left[-\frac{1}{2}\nabla^2 + V(r)\right]\Psi_{nk}(r) + \int dr'\Sigma(r,r';E_{nk})\Psi_{nk}(r') = E_{nk}\Psi_{nk}(r)$$

(Equation 2.13)

The above equation is like the KS equation, except that V_{xc} is replaced by a non-local, non-hermitian electron self-energy operator, $\Sigma(r,r';E_{nk})$. The self-energy operator is given within Hedin's GW approximation [26,27] as follows:

$$\Sigma = iGW \qquad \text{(Equation 2.14)}$$

wherein, W is screened Coulomb interaction, and G is the single-particle Green's function. W is calculated from the inverse dielectric function and bare Coulomb interaction, V, as follows:

$$W(q,\omega) = \varepsilon^{-1}(q,\omega)V(q+G') \qquad \text{(Equation 2.15)}$$

The time-ordered Green's function is the central tool in this approach and its physical interpretation is that of a creation and annihilation of electron and hole at time t and position r. In a practical calculation, it is a propagator constructed from single particle energies ε_{nk} and

wavefunctions Ψ_{nk}.

$$G(r,r',E) = \sum_{nk} \frac{\Psi_{nk}(r)\Psi_{nk}^{*}(r')}{E-\varepsilon_{nk}-i\delta_{nk}} \qquad \text{(Equation 2.16)}$$

The real part of self-energy operator can be decomposed into two parts:

$$Re\Sigma = \Sigma_{SX} + \Sigma_{CH} \qquad \text{(Equation 2.17)}$$

Here, the screened exchange term Σ_{SX} represents poles in the Green's function and the Coulomb hole part Σ_{CH} is for poles in the screened Coulomb interaction, W.

Initially DFT-LDA values (mean-field eigenfunctions and eigenvalues) are taken as the input to calculate G as per Equation 16 and W using Equation 15. For practical purposes, a semi-self-consistent calculation is undertaken wherein, only the energies for G are iterated whereas the time-consuming screening interaction 'W' remains the same as calculating the dielectric matrix. This is the so called GW_0 calculation [28].

2.3 Bethe-Salpeter Equation

Absorption spectrum, especially in reduced dimensional materials is dominated by excitonic effects. BSE – a two particle Green's function equation is employed. It is also an eigenvalue equation, given as follows:

$$(E_{ck} - E_{vk})A_{vck}^{S} + \sum_{v'c'k} K_{vck,v'c'k}^{eh} A_{v'c'k}^{S} = \Omega_S A_{vck}^{S} \qquad \text{(Equation 2.18)}$$

where, E_{ck} and E_{vk} are quasi-electron and quasi-hole states. Ω_S and A_{vck}^{S} are the exciton energy and amplitude of excitonic state S. Within the Tam Dancoff approximation [29], excitonic states are written as linear superpositions of electron and hole states:

$$S(e,h) = \sum_{v}^{occ} \sum_{c}^{empty} A_{vc}^{s} \Phi_c \Phi_v^{*} \qquad \text{(Equation 2.19)}$$

In Equation 2.18, K^{eh} is the interacting electron hole kernel, which can be separated into two parts:

1) A direct attractive term Kd which is dependent on screened coulomb interaction W.
2) An exchange term Kx describing the repulsive interaction between e-h pairs.

The absorption spectrum is the imaginary part of the dielectric function $\varepsilon_2^0(\omega)$. Without the electron-hole interaction, it is given as follows:

$$\varepsilon_2^0(\omega) = \frac{16\pi e^2}{\omega^2}\sum_{v,c}|\lambda < v|v|c > |\delta(\omega - (E_c - E_V)) \qquad \text{(Equation 2.20)}$$

Where the oscillator strength is derived from Fermi's golden rule, v is velocity operator, λ is the wave vector pointing in the direction of light. Considering the interacting electron-hole picture or considering electron hole interaction, we have:

$$\varepsilon_2^0(\omega) = \frac{16\pi e^2}{\omega^2}\sum_{S}|\lambda < 0|v|S > |\delta(\omega - \Omega_s) \qquad \text{(Equation 2.21)}$$

The major difference between the non-interacting and interacting frameworks stems from the fact that in Equation 20 the oscillator strength is a summation over vertical transitions of single particle states, whereas while incorporating the excitonic effects, it is a summation over excitonic states S. Also, the former equation is a delta function of difference between input photon energy and the band gap, whereas in the interacting case it is a difference between incoming photon energy and exciton binding energies Ω.

An exciton is like a hydrogen atom problem, which can be solved analytically to obtain excitonic energy eigen functions and exciton energy in the form of Rydberg series. Within the effective mass approximation, exciton binding energy is obtained as follows:

$$E_b = \frac{\mu}{\varepsilon n^2} \qquad \text{(Equation 2.22)}$$

where, μ is the reduced effective mass of electron-hole pair, ε is dielectric screening and n is for the n^{th} energy level.

Chapter 3: Computational Details

The GW-BSE method is the most widely adopted technique to compute the GW-corrected electronic structure and excited state properties of materials. The drawback is that it is computationally very expensive. The method as implemented by Hyberstein and Louie was used in the BerkeleyGW package [30], which was intended to be executed on top of other mean field codes such as Quantum Espresso [31]. The whole process can be divided into three main steps:

1) DFT calculations using Quantum Espresso;
2) Electronic structure or ground state properties using epsilon.x and sigma.x executable from the BGW package; and,
3) Calculating optical or excited state properties using Kernel.x and absorption.x executables.

3.1 Mean Field Calculations

All the mean-field calculations using PBE-DFT were done using the Quantum Espresso package. The recent 'opt-BK86' type of van der Waal's functional [32-35] was used as input DFT functional. A hexagonal unit cell with $a = b \neq c$ was employed for mean field calculations and a tetragonal box with $a = b \neq c_{chain}$ was selected for Se and Te atomic chains. The vacuum surrounding the atomic chains in the XY-plane was kept large enough so that 99% of charge density falls within half the size of unit cell. This was calculated using surface.x feature of BGW package. Crystalline axis 'c' was optimized at its true ground state. As shown in Figures 3.1 and 3.2, the 'c-axis' for Se and Te was 4.95 Å and 5.6 Å , respectively. The exfoliation energy, E_{exf} was obtained as a difference in ground state energy of bulk system and a single helical chain. Inclusion of van der Waal's interaction had a significant effect on E_{exf}. But, in both the cases it was higher for Te as compared to Se with 0.547 for Se and 0.926 for Te nanowires.

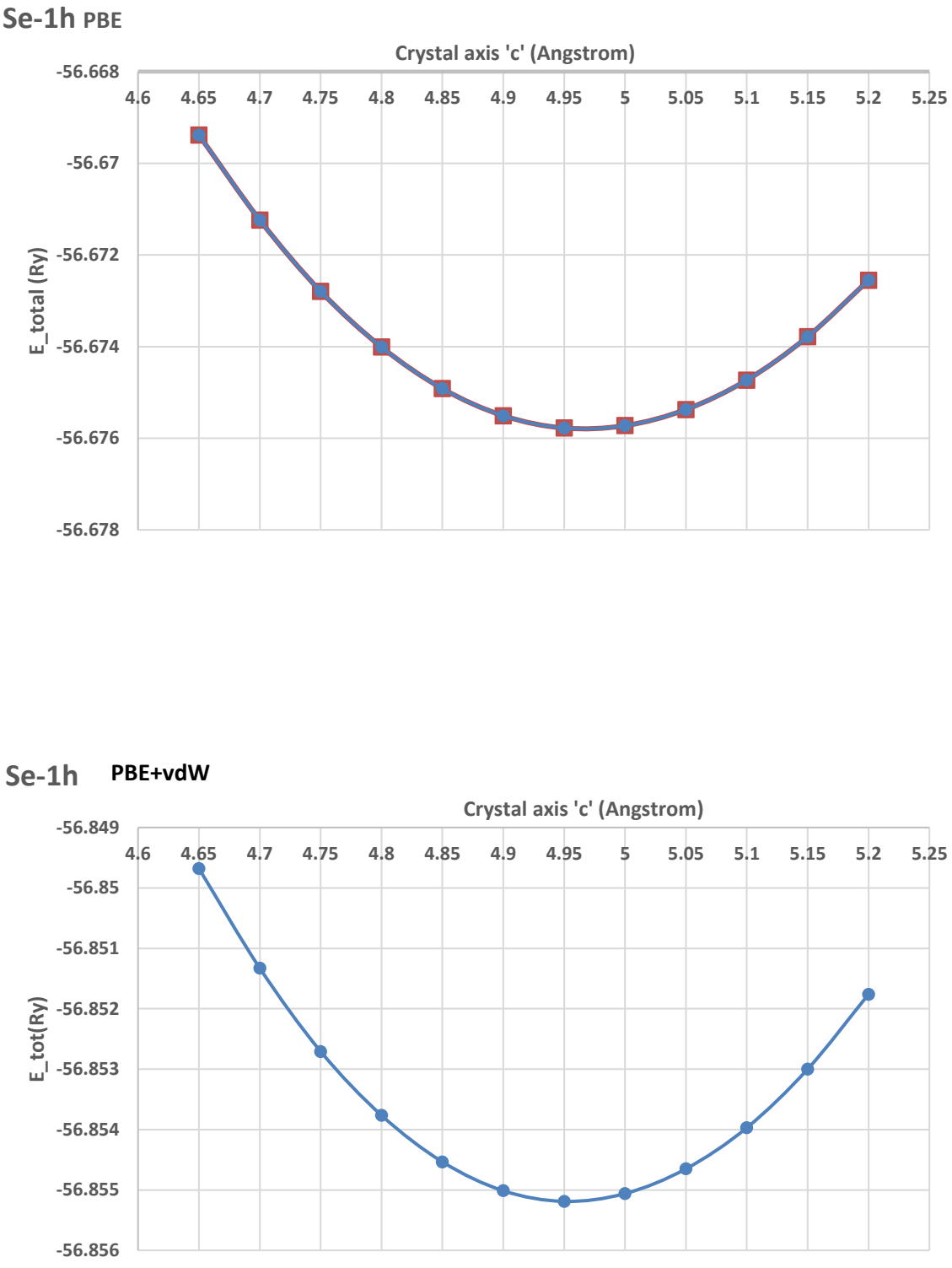

Figure 3.1 Ground state Energy Vs. crystalline axis 'c' with and w/o vdW's correction for Se atomic chain.

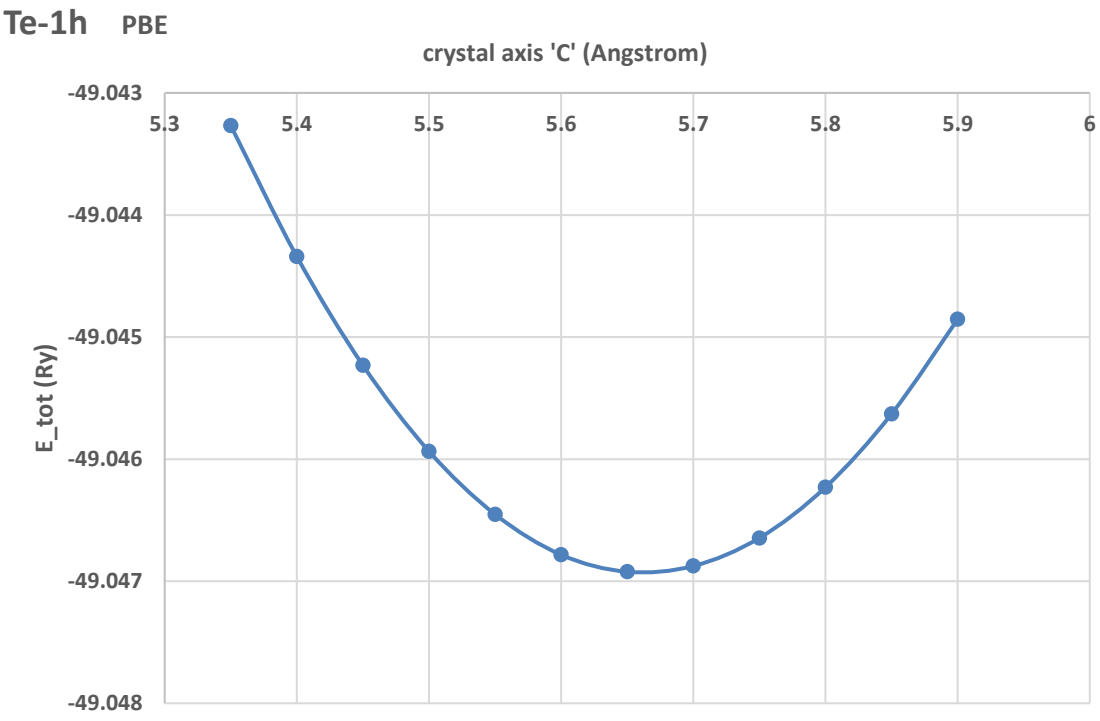

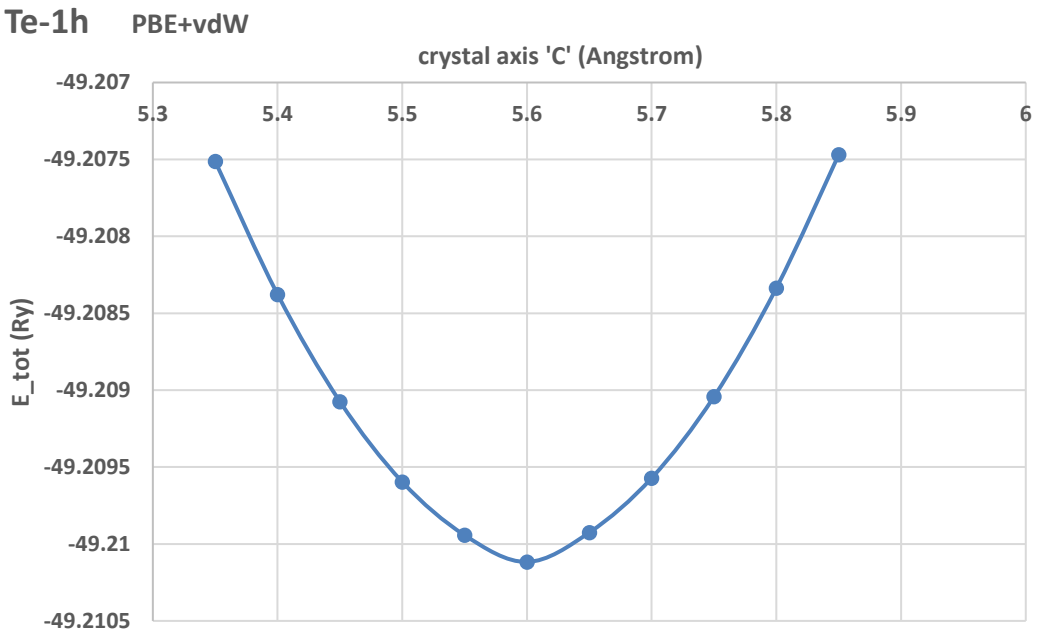

Figure 3.2 Ground state energy Vs. crystalline axis 'c' with and w/o vdW's correction for Te atomic chain.

A $1 \times 1 \times 20$ k-points grid with c-axis as periodic direction was chosen for single helical chains. K-points were generated using the kgrid.x executable from the BerkeleyGW package. A cutoff for the plane wave basis set of 45 Ry and 85 Ry was employed for Se and Te to achieve convergence. Norm-conserving pseudopotential of the Troullier-Martin's type was used [36]. As the name suggests, it enforces the condition that beyond a certain cut-off radius, the norm of pseudo wavefunctions is the same as its corresponding all electron wave-function. In general norm-conserving pseudopotential possesses following properties:

1. The valence pseudo-wavefunction generated contains no nodes. It is a smooth wave-function which can be expanded by a smaller number of plane waves.
2. The radial part of normalized pseudo wavefunction is same as the radial part of all-electron wave function, beyond the critical radii, r_{cl}.
3. Both possess identical charge density within r_{cl}.

The final step at the mean field level is to convert the generated wavefunctions to a BGW readable format using a post processing feature of quantum Espresso, called pw2bgw.x. It requires a minimum of four mean field calculations with varying kgrid and q-shift: WFN or WFN_co (WFN Coarses), a q-grid shifted WFNq, a finer K-mesh – WFN_fi with larger number of k-points for higher precession and a shifted finer WFNq_fi. It is important to note that both, the lattice vectors and atomic co-ordinates are having the same unit in the input file before generating the K-points. The FFT grid should be exactly supplied from the output of scf calculations. Also important is to use same version of QE for scf and pw2bgw.x steps before the BGW readable WFN is calculated.

3.2 GW-BSE Calculation

A typical BGW algorithm is shown in the flowchart in Figure 3.3 given below:

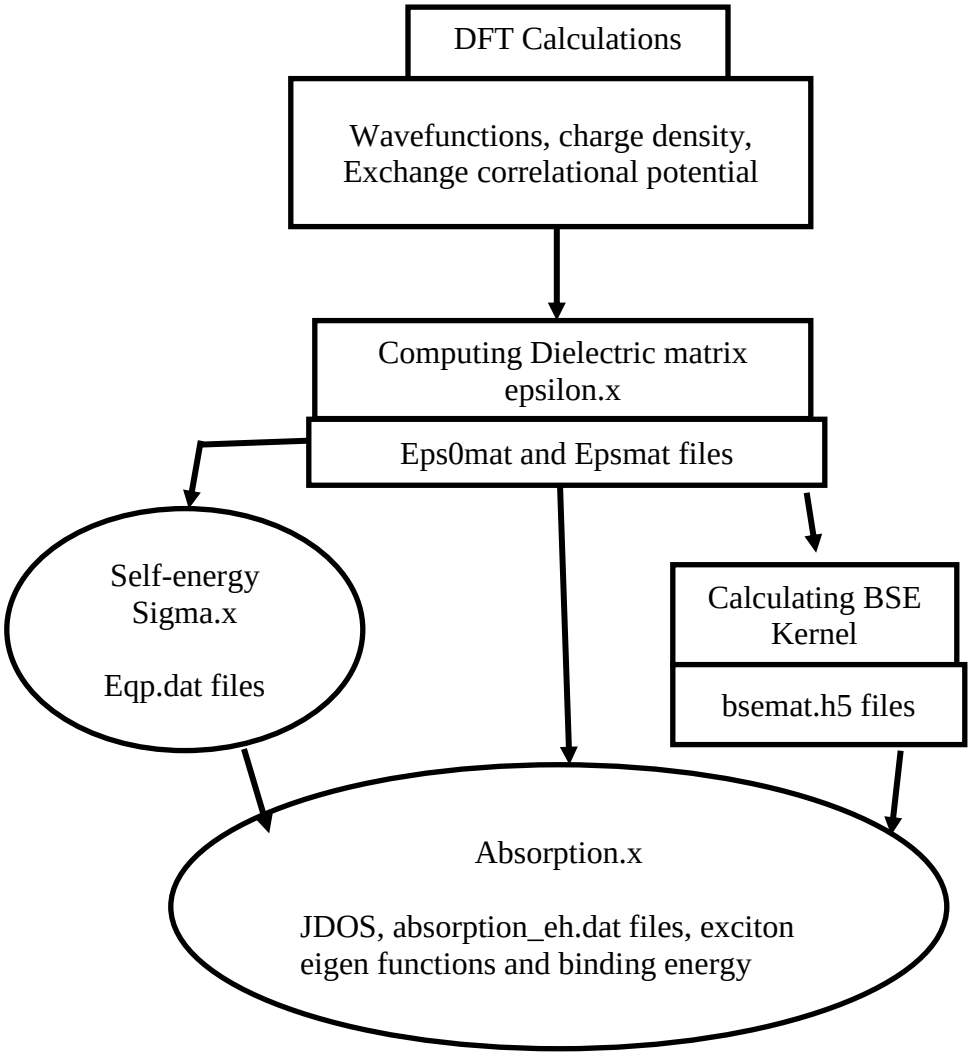

Figure 3.3 Berkeley-GW Algorithm.

The first step is using epsilon.x executable to calculate the dielectric function and inverse of it before calculating screened interaction, W. It takes a coarse wavefunction k-points as input q-points, with the exception that the first k-point is shifted slightly away from gamma, so that there is no divergence in calculations. Due to spatial non-locality and frequency dependence of epsilon, it is a computationally expensive step. One often relies on the plasmon pole

approximation: i.e., that the dielectric function is flat, except for poles at plasma frequency ω_p with other constraints to obtain the oscillator strength in the static limit. Two different types of GPP models have been used here: Hybertsen Louie (HL) and Godby-Needs (GN) GPP models. It is advantageous to use GN GPP model as it calculates the dielectric matrix using both imaginary and real axis, while HL imposes the normalized f-sum rule. It is also more accurate and closer to numerical integration technique and experimental data [37]. A cell wire truncation input flag was used to avoid the spurious interactions between the neighboring unit cells for a single helical chain. The output files eps0mat.h5 and epsmat.h5 were used to calculate screened interaction, W, to obtain electron self-energy corrections in the next step.

In the "sigma" executable, the screened Coulomb interaction W was calculated from the inverse dielectric matrix and Green's function, using mean-field eigenfunctions and eigenenergies. The self-energy operator was then calculated and diagonalized in the mean-field basis. Then the BSE executable kernel wrote bsemat.h5 files as an output. The absorption executable used the bsemat matrices along with WFN files from coarser and finer grids. The BSE Hamiltonian was diagonalized yielding excitonic wavefunctions and eigenenergies.

3.3 Convergence tests

It is highly significant to check convergence of GW-BSE results with respect to various parameters such as the k-grid, the number of conduction bands and, most importantly, the screened coulomb interaction cutoff for calculating the dielectric matrix. For a small system of three atoms, a sufficiently large k-grid of 30 k-points along the z-axis was employed. Through initial tests, it was found that quasi-particle energy eigen-values were constant with respect to the number of unoccupied bands. As shown in the Figures 3.4a and b and 3.5a and b, convergence was achieved with a cutoff as high as 20 Ry for Hybertsen Louie plasmon pole model, and 15 Ry

for Godby Needs plasmon pole model.

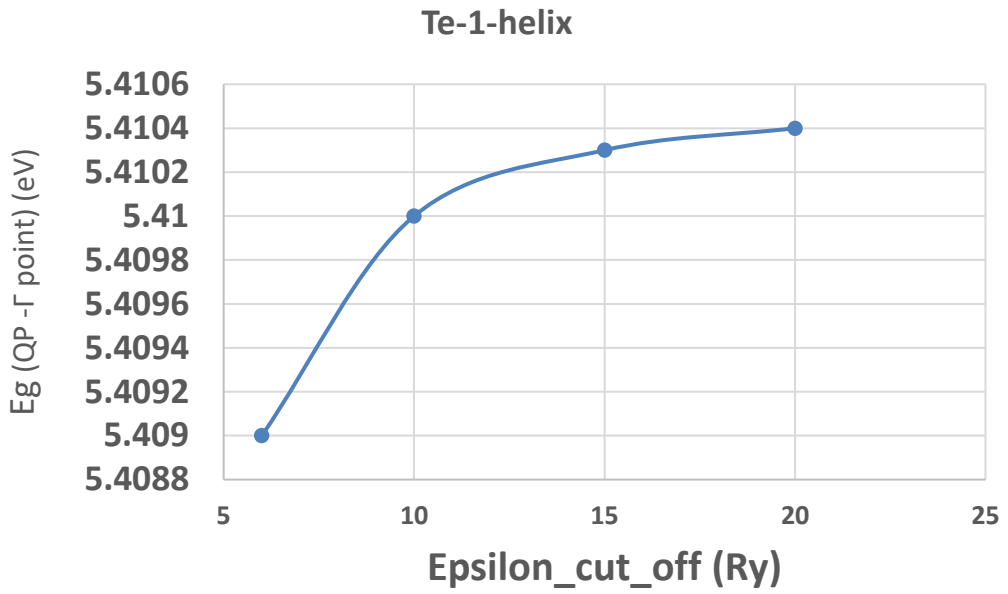

Figure 3.4a Convergence at gamma point w.r.t epsilon kinetic energy cut_off for Te atomic chain.

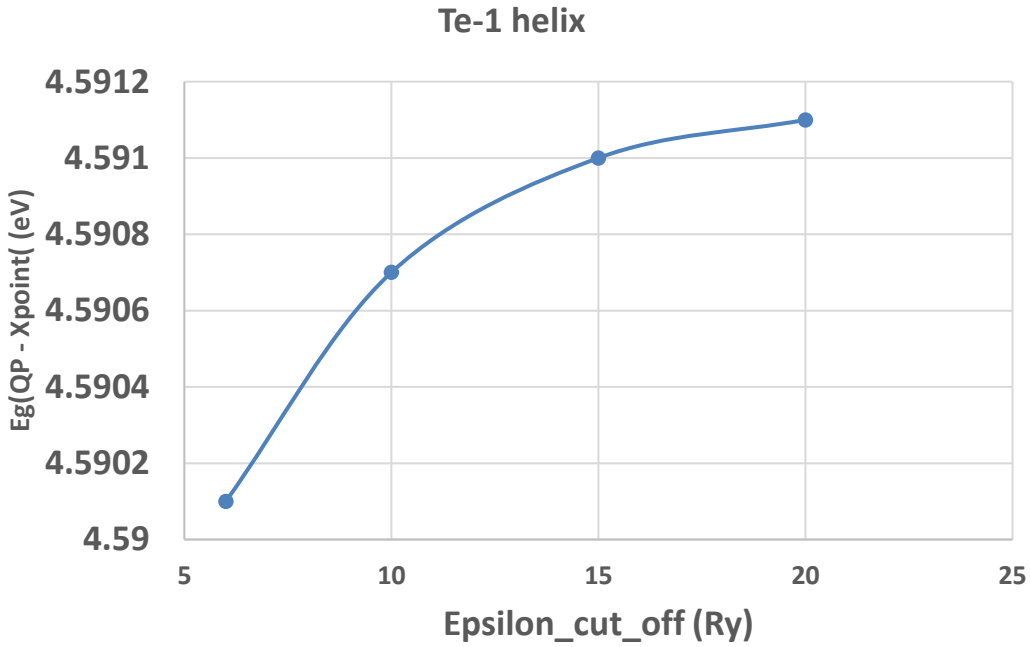

Figure 3.4b Convergence at X point w.r.t epsilon Kinetic energy cut_off for Te atomic chain.

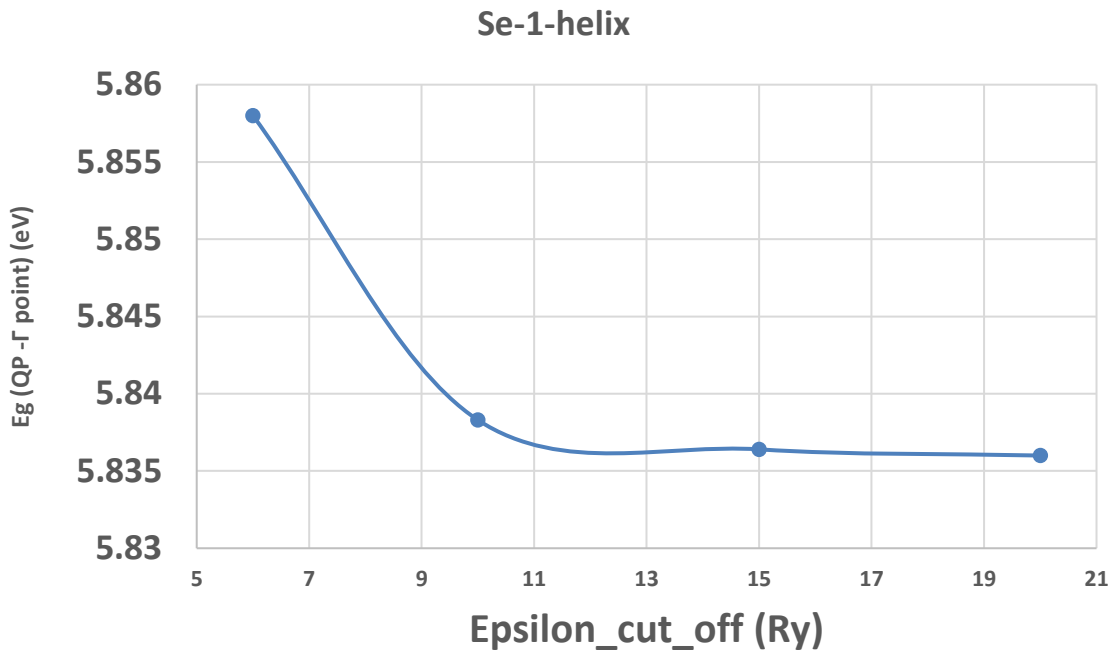

Figure 3.5a Convergence at gamma point w.r.t epsilon Kinetic energy cut_off for Se atomic chain.

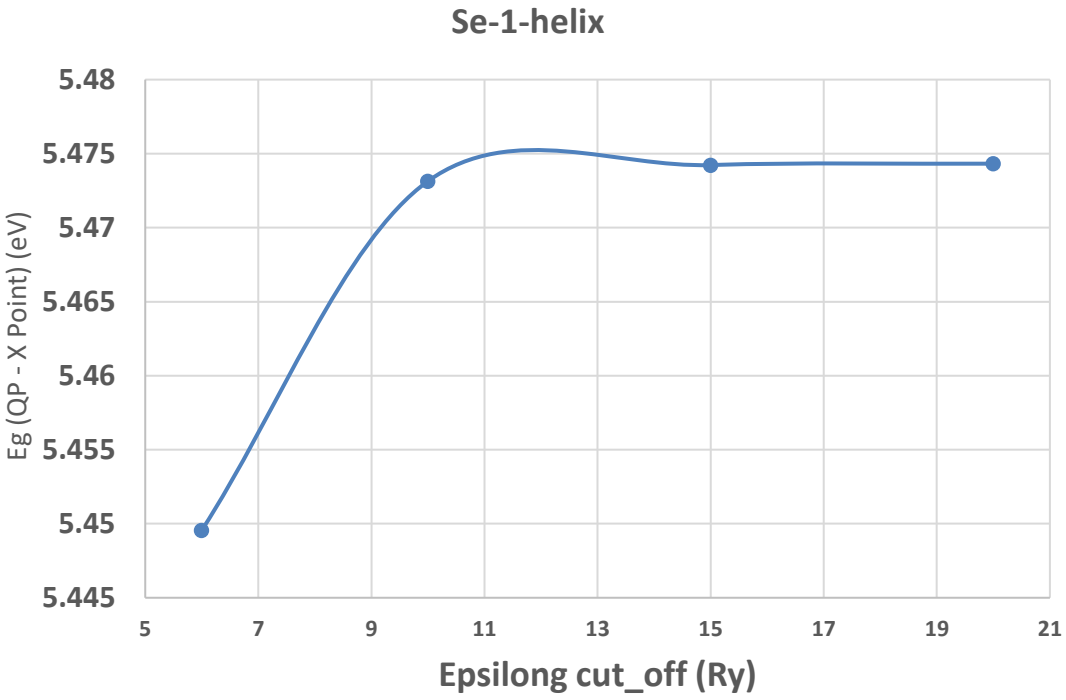

Figure 3.5b Convergence at X point w.r.t. Kinetic energy cut_off for Se atomic chain.

Chapter 4: Electronic Properties of Se and Te Nano-Wires

4.1 Mean-Field Band Structure

At the mean field level, the electronic structure computed for single helical chains was interpolated on a 1×1×30 k-point grid. As shown in Figure 4.1a and 4.1b, the electronic band structures were calculated along the high symmetry k-points Γ to X of the first Brillouin zone.

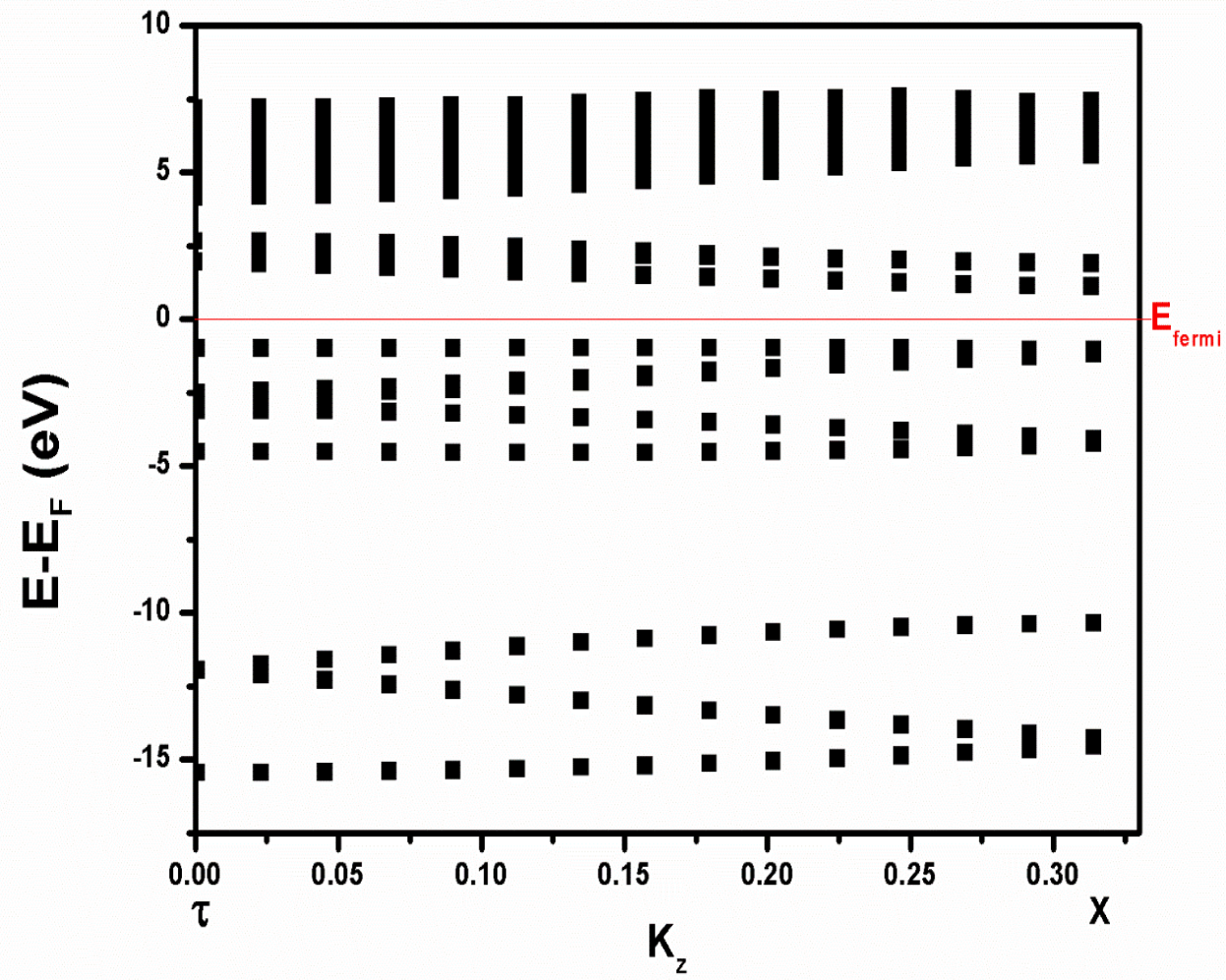

Figure 4.1a Mean field band structure for Se atomic chains.

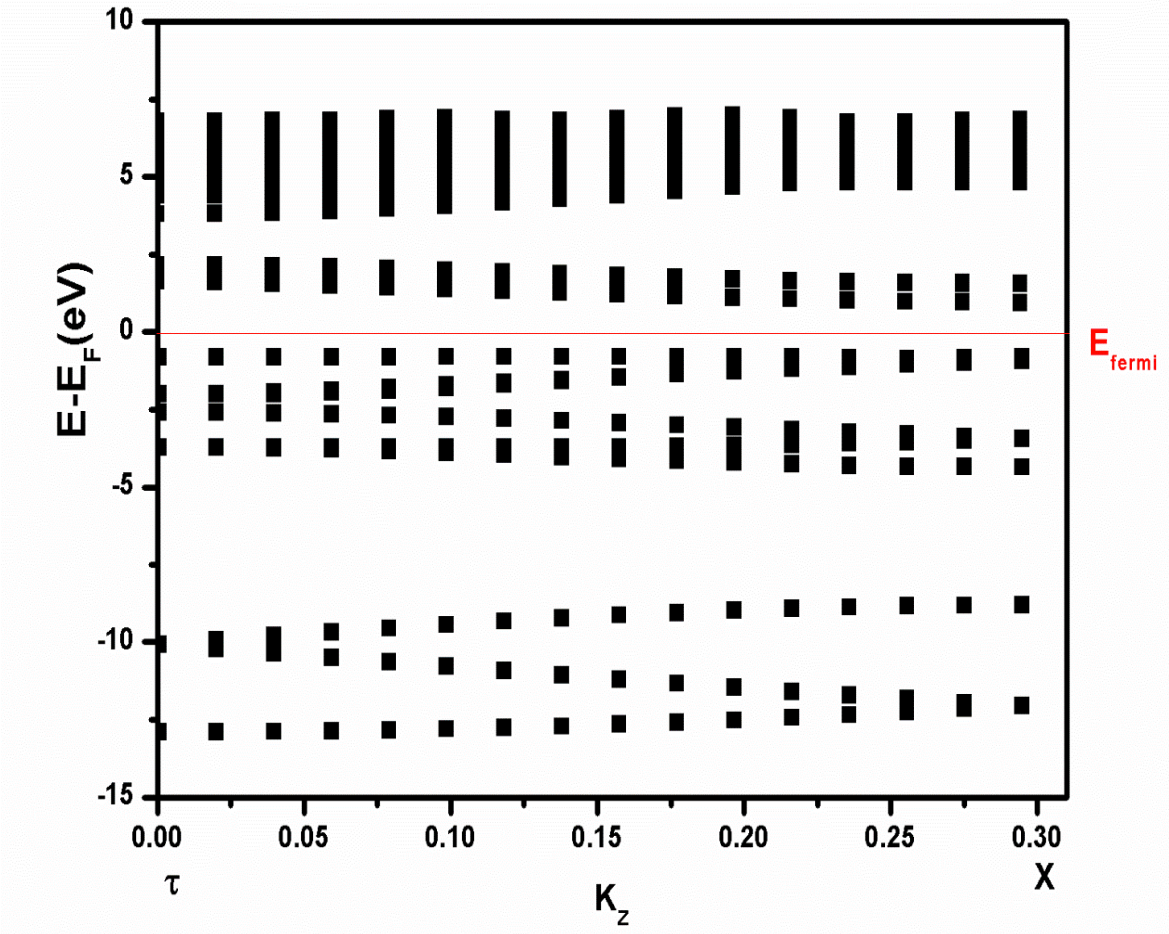

Figure 4.1b Mean field electronic structure of Te single helical chains.

4.2 Quasi-particle band structure:

As shown in Figure 4.2a and 4.2b, GW corrected quasi-particle corrections to the DFT energy eigenvalues obtained in a semi self-consistent scheme widens the electronic band gaps. It is calculated using both, HL and GN GPP models. The band gap for Se is 5.22 eV using GN GPP model and 5.47 eV for HL GPP. Similarly for Te, the highest value of Eg is 4.59 with HL GPP model and 4.44 eV with GN GPP model. Se is predicted to be an indirect band gap semiconductor as per the previous mean-field corrections whereas GW calculations yields the true material proeprty,as per which, Se is a direct band gap semiconductor.

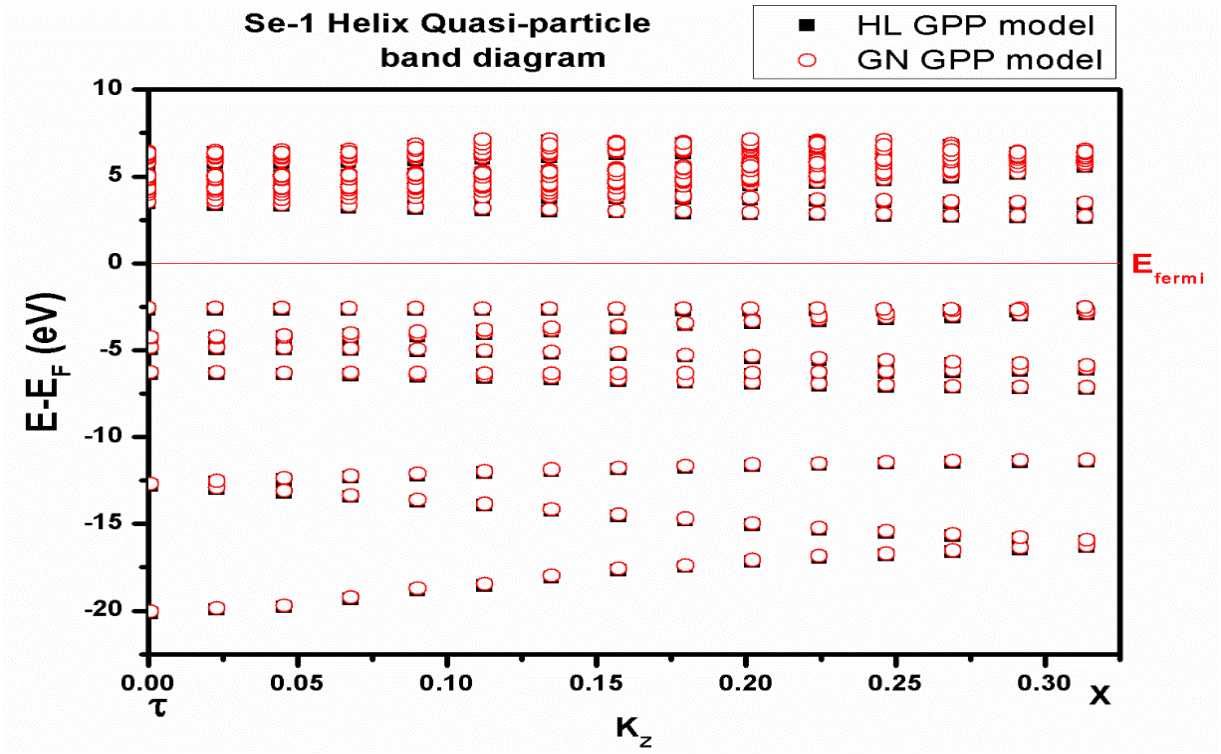

Figure 4.2a Quasi-particle band structure of Se single helical chains.

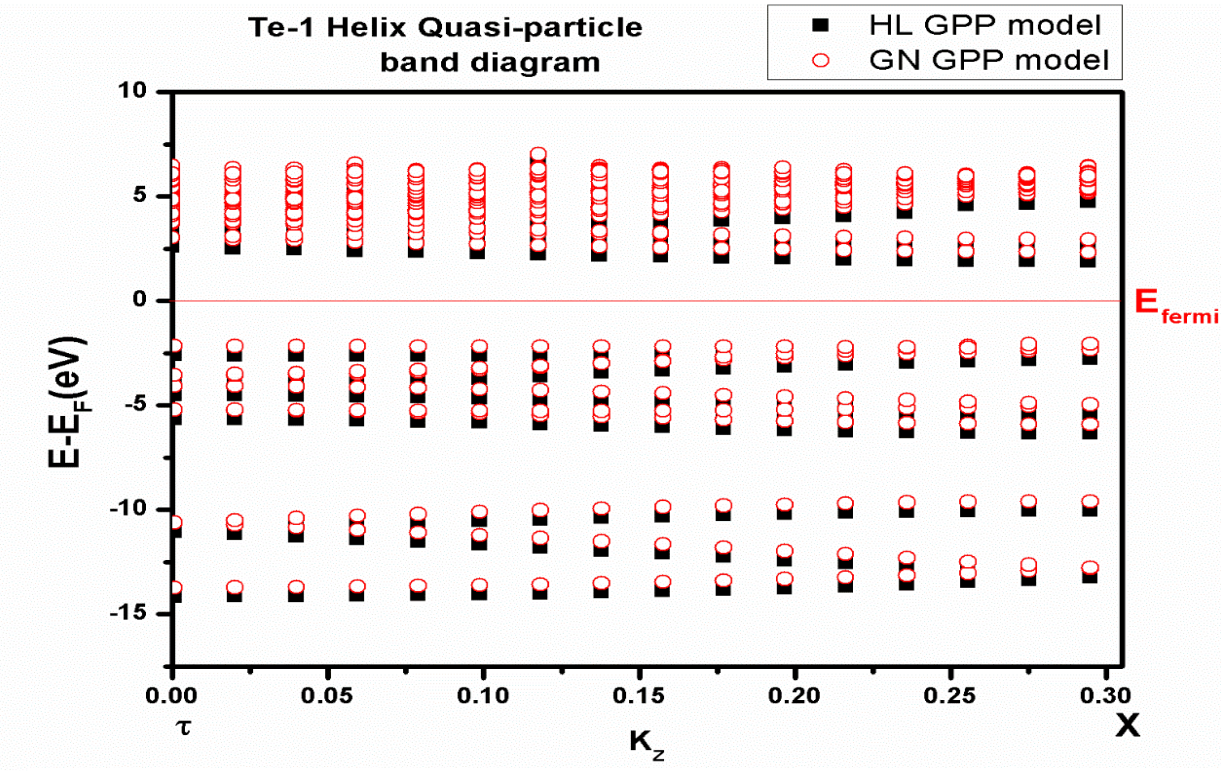

Figure 4.2b Quasi-particle band structure of Te single helical chains.

Chapter 5: Optical Properties of Se and Te Nano-Wires

Absorption spectrum was obtained from imaginary part of macroscopic dielectric function as a function of incoming photon energy. As shown in the Figure 5.1a and 5.1b, both types of GPP models were employed separately to calculate absorption spectrum with and without electron hole interactions. For both Se and Te, there are two bound excitonic peaks, labeled as 1 and 2 and remaining are resonant excitons whose binding energy falls within the quasi-particle band gap. The tentative difference between the peaks labeled as 1 and 1' and 2 and 2' gives the exciton binding energy.

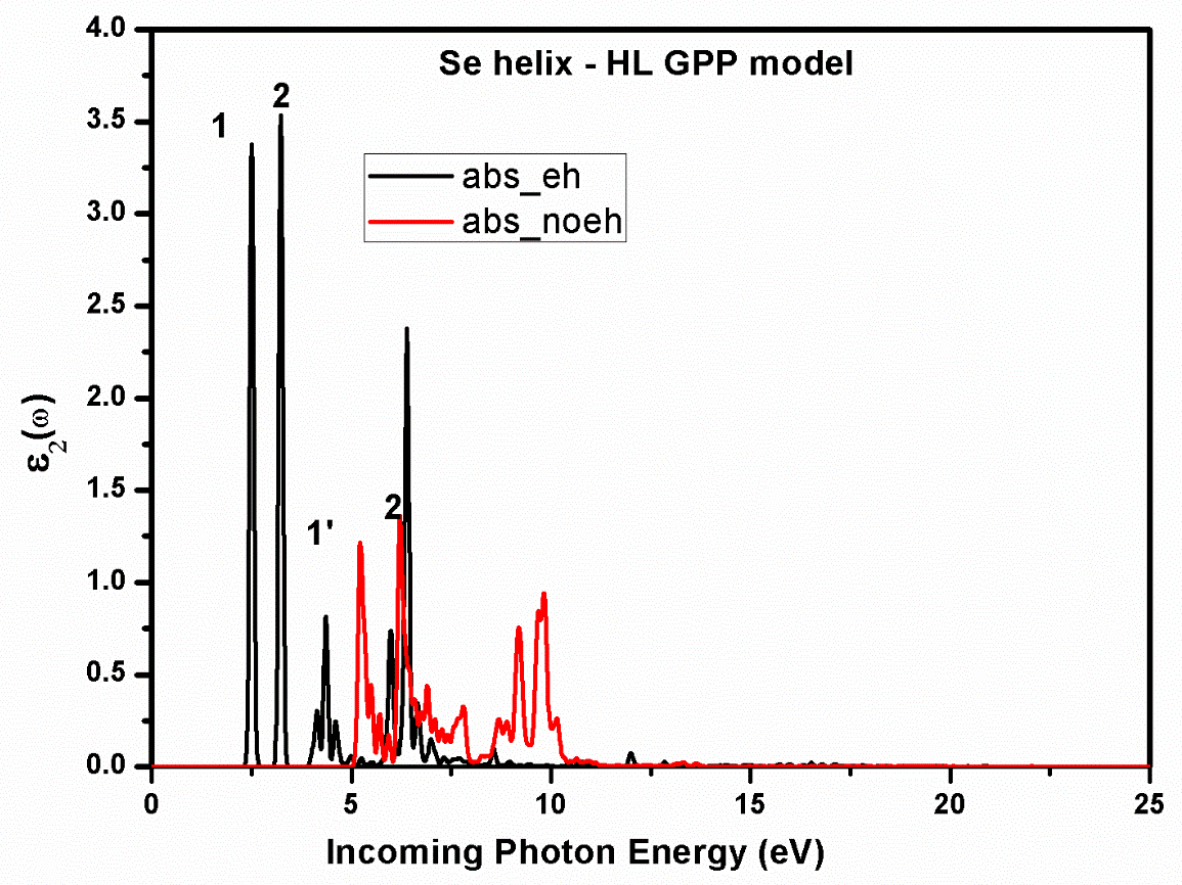

Figure 5.1a Absorption spectrum of Se atomic chains with (black line) and without (red line) electron hole interaction within the Hybertsen-Louie GPP model.

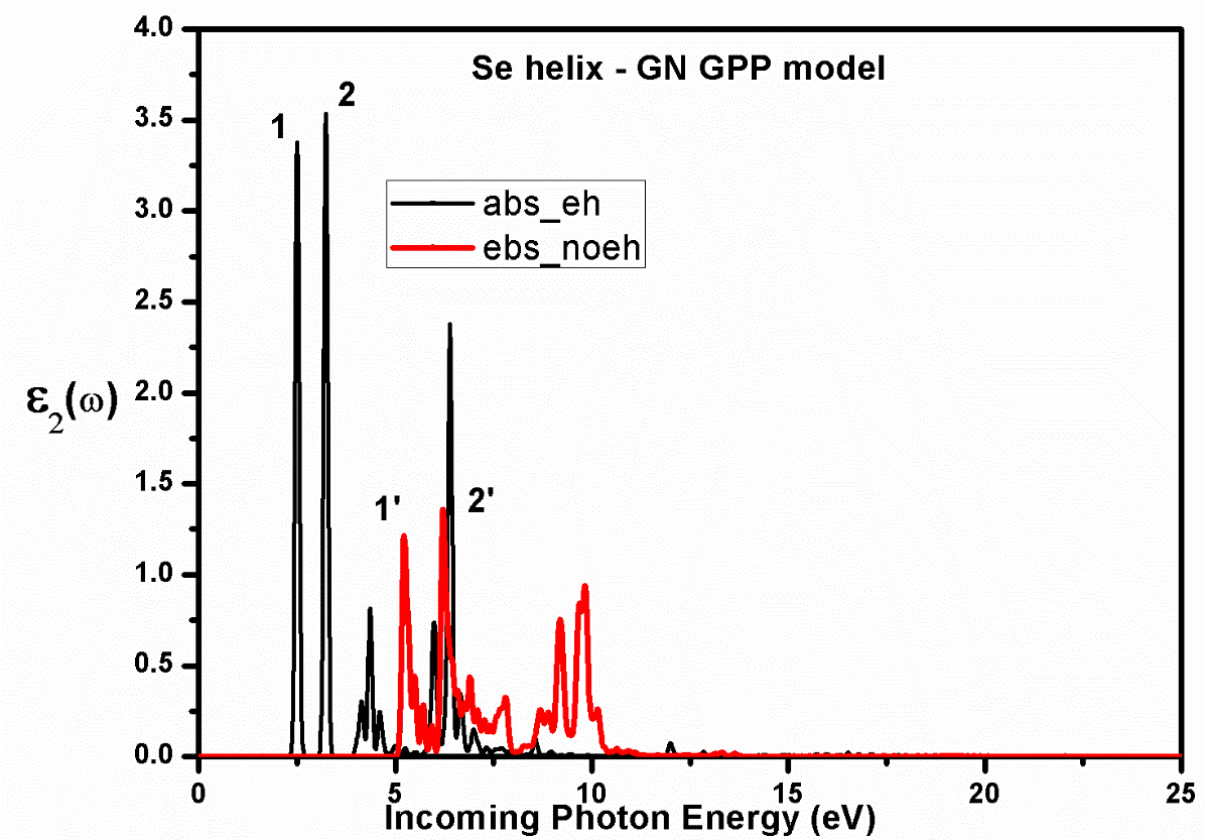

Figure 5.1b Absorption spectrum of Se atomic chains with (black line) and without (red line) electron hole interaction within the Godby Needed's GPP model.

Similarly, we have simulated the absorption for Te single helical chains, as shown in Figure 5.2a and 5.2b, with HL and GN GPP, respectively. As per Equation 2.20, the absorption spectrum without e-h interaction (red curve) is proportional to delta function of difference between incoming photon energy and GW corrected band gap. Since the intensity of interacting electron-hole spectrum is higher as compared to the non-interacting curve the direct part of Bethe-Salpeter kernel which is proportional to screened coulombic interaction 'W' is dominant (which is generally the case with reduced dimensional semiconductors).

The first bound exciton for Se and Te is highly localized along the crystalline c-axis. For instance, Figure 5.3 shows excitonic wave function for Se using HL GPP model in real space. The square of excitonic wave function's amplitude $|A^{s}_{vck}|^2$ along the crystalline 'c-axis' is

shown.

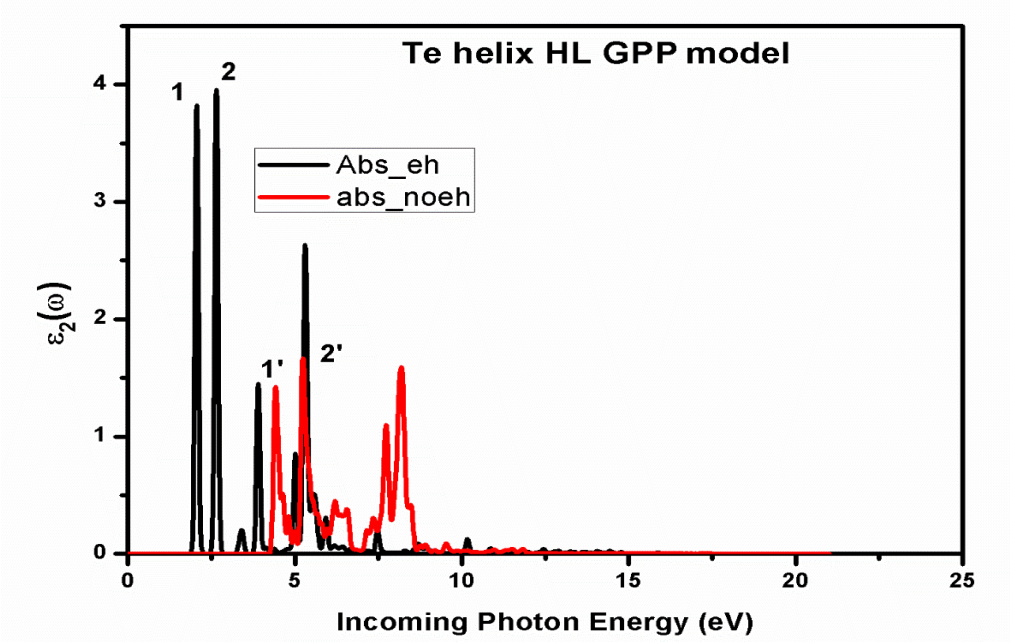

Figure 5.2a Absorption spectrum of Te atomic chains with (black line) and without (red line) electron hole interaction within the Hybertsen-Louie GPP model.

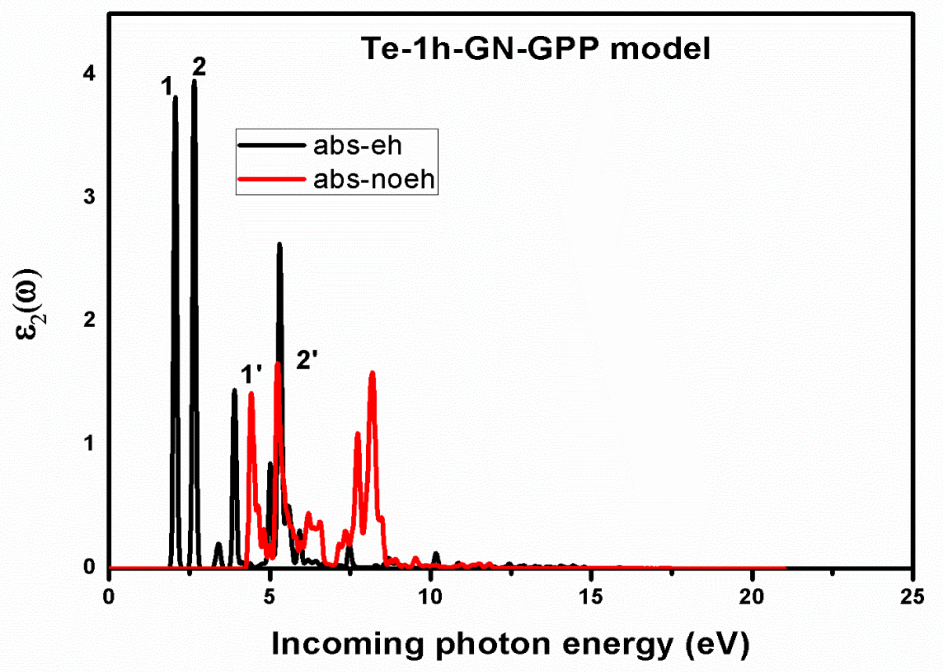

Figure 5.2b Absorption spectrum of Te atomic chains with (black line) and without (red line) electron hole interaction within the Godby-Needs GPP models.

Figure 5.3 exciton wave function for Se single helical chain.

Chapter 6: Conclusion

It has been shown that single helical chains of Se and Te can be used for operating in the Vis-range for optoelectronic devices. High exciton binding energy computed using both types of GPP models shows its prominence for fabricating mixed dimensional van der Waal's heterostructures, especially excitonic interconnects with anisotropic 2D semiconductors.

Bulk Se and Te exhibits a high magnitude non-linear optical response. Thus, one can expect a more enhanced response for such single helical chains due to quantum confinement in 1D. It is crucial to theoretically investigate their third order non-linear optical response using the rudimentary form of Berkeley-GW code, in the future. Another important aspect for pragmatic applications is to simulate its thickness or diameter dependent electronic and excitonic properties. Further, one needs to study its stability in air and humid atmosphere. One can use molecular dynamics to study the dynamics of oxidation for such Se and Te single helical chains and larger diameter wires.

References:

1) H. M. Gibbs, S. S. Tarng, J. L. Jewell, D. A. Weinberger, and K. Tai, Appl. Phys. Lett. 41, 221 (1998).

2) E. V. Calman, M. M. Fogler, L. V. Butov, S. Hu, A. Mishchenko and A. K. Geim, Nat. Commun., 9,1895 (2018).

3) M. Baldo and V. Stojanovic, Nat. Photon.,3, 558 (2009).

4) D. Jariwala, T. J. Marks and M. C. Hersam, Nat. Mater., 16,170 (2017).

5) V. Negoita , D. W. Snoke and K. Eberl, Phys. Rev. B., 60, 4 (1999).

6) H. Cruz, J. Appl. Phys. 113, 153706 (2013).

7) M. M. Ugeda, A. Bradley, S. Shi, F. H. da Jornada, Y. Zhang, D. Y. Qiu, W. Ruan, S. Mo, Z. Hussain, Z. Shen, F. Wang, S. G. Louie & M. F. Crommie, Nat Mater.,13,1091 (2014).

8) K. F. Mak, K. He, C. Lee, G. H. Lee, J. Hone, T. F. Heinz & J. Shan, Nat. Mater., 12, 207(2013).

9) E. Chang, G. Bussi, A. Ruini, and E. Molinari, Phys. Rev. Lett. 92, 196401 (2004).

10) V. Perebeinos, J. Tersoff, and P. Avouris, Phys. Rev. Lett. 92, 257402 (2004).

11) M. Bruno, M. Palummo, A. Marini, R. Sole, and S. Ossicini , Phys. Rev. Lett. 98, 036807, (2007).

12) D. A. Wheeler, J. Huang, R. J. Newhouse, W. Zhang, S. Lee, and J. Z. Zhang, J. Phys. Chem. Lett.,3 (6), 766–771, (2012).

13) C. D. Spataru, S. Ismail-Beigi, L. X. Benedict, and S. G. Louie Phys. Rev. Lett. 92, 077402, (2004).

14) G. Samsonidze, F. J. Ribeiro, M. L. Cohen, and S. G. Louie, Phys. Rev. B 90, 035123, (2014).

15) M. Rohlfing and S. G. Louie, Phys. Rev. Lett. 82, 1959 (1999).

16) C. H. Park, C. D. Spataru, and S. G. Louie, Phys. Rev. Lett. 96, 126105 (2006).

17) M. Bruno, M. Palummo, A. Marini, R. Del Sole, V. Olevano, A. N. Kholod, and S. Ossicini, Phys. Rev. B 72, 153310 (2005).

18) E. Andharia, T. P. Kaloni, G. J. Salamo, S. Yu, H. O. H. Churchill, and S. B. Lopez, Phys. Rev. B 98, 035420 (2018).

19) D. J. Olechna and R. S. Knox, Phys. Rev. 140, A986 (1965).

20) M. U. Kahaly, P. Ghosh, S. Narasimhan, and U. V. Waghmare, J. Chem. Phys. 128, 044718 (2008).

21) P. Ghosh, M. U. Kahaly, and U. V. Waghmare, Phys. Rev. B 75, 245437 (2007).

22) G. Kresse and J. Furthmuller, Phys. Rev. B, 54, 11169 (1996).

23) B. Tuttle, S. Alhassan, and S. Pantelides, Nanomaterials, 7, 115 (2017).

24) P. Hohenberg and W. Kohn, Phys. Rev., 136(3B): B864–B871(1964).

25) K. Walter and S. Lu Jeu, Physical Review. 140 (4A): A1133–A113, (1965).

26) L. Hedin, Phys. Rev. 139, A796 (1965).

27) L. Hedin and S. Lundqvist, Solid State Phys. 23, 1 (1969).

28) Y. Liang, Washington University Open Scholarship, *All Theses and Dissertations (ETDs)*. 1317 (2014). (http://openscholarship.wustl.edu/etd/1317)

29) S. Okubo., Progress of Theoretical Physics, 12(5):603‑622, 1954.

30) J. Deslippe, G. Samsonidze, D. A. Strubbe, M. Jain, M. L. Cohen, and S. G. Louie, Comput. Phys. Commun. 183, 1269 (2012).

31) P. Giannozzi, S. Baroni, N. Bonini, M. Calandra, R. Car, C. Cavazzoni, D. Ceresoli, G. L. Chiarotti, M. Cococcioni and I. Dabo, J. Phys. Condens. Matter 21, 395502 (2009).

32) T. Thonhauser, V. R. Cooper, S. Li, A. Puzder, P. Hyldgaard, and D. C. Langreth, Phys. Rev. B 76,125112 (2007).

33) D. Langreth, B. I. Lundqvist, S. D. Chakarova-Kack, V. Cooper, M. Dion, P. Hyldgaard, A. Kelkkanen, J. Kleis, L. Kong and S. Li, J. Phys. Condens. Matter 21, 084203 (2009).

34) T. Thonhauser, S. Zuluaga, C. Arter, K. Berland, E. Schroder, and P. Hyldgaard, Phys. Rev. Lett. 115,136402 (2015).

35) K. Berland, V. R. Cooper, K. Lee, E. Schroder, T. Thonhauser, P. Hyldgaard, and B. I. Lundqvist, Rep. Prog. Phys. 78, 066501 (2015).

36) N. Troullier and J.L. Martins, Phys. Rev. B 43, 1993 (1991).

37) P. Larson, M. Dvorak, and Z. Wu, Phys. Rev. B 88, 125205 (2013).

Appendix A: Description of Research for Popular Publication

When an electron is excited to the conduction band by a photon, it creates a hole in the valence band. Such a pair of electron and hole is bound by attractive Coloumb interaction. Such a bound electron-hole pair is called as an exciton. An exciton forms an intermediate quasi-particle that can be used to fabricate excitonic interconnects between optical waveguides for signal transmission and transistors for signal processing. Such excitonic devices will proffer a high switching speed, signal to noise ratio, and more compact and miniaturized devices. Excitonic devices will require a high exciton binding energy and radiative lifetime for its successful operation, which depends on quantum confinement. Exciton binding energy increases as one goes from 3-dimension to 2-dimension and 1-dimension quantum confined nanostructures.

For 1D nanostructures, as the confinement length decreases, exciton binding energy increases, due to reduced dielectric screening and enhanced effective mass arising from less disperse and more flat bands. As compared to conventional group IV/V based GaAs/AlGaAs based quantum wells and wires, the confinement length in such van der Waal's (vdW's) structure is an order less viz., 4.5 Å to 5.5 Å as compared to 4 nm to 5 nm for quantum wells (QWLs) and quantum wires (QWRs).

As compared to conventional Density Functional Theory (DFT) technique which employs a semi-classical variable electron density, we use a heterodox technique relying on many-body perturbation effects which account for electron self-energy within GW approximation, where 'G', Green's Function, is a propagator describing the creation and annihilation of electron-hole pairs and 'W' is reduced screening effects. Not only does it enlarge the electronic bandgap, with more accurate values that are closer to experimental results, but it

predicts the material to be a direct band-gap semiconductor.

Further, the optical properties are obtained by solving Bethe-Salpeter equation and exciton wave function is plotted in real space. The high exciton binding energy for Se and Te single helical chains has been investigated for the first time. They can be used to form excitonic interconnects and all-optical transistors operating at room temperature.

Appendix B: Executive Summary of Newly Created Intellectual Property

The following list of new intellectual property items were created in the course of this research project.

1) The excitonic properties of Se and Te single helical chains have been investigated theoretically,
2) A GW corrected band gap using partial self-consistency with accurate output has been calculated. (Use of optimum vacuum along the XY-plane and more recent vdW's functional has been used.)
3) A tentative estimate of exfoliation energy required to mechanically exfoliate such single helical chains has been presented to bolster experimental research.

Appendix C: Potential Patent and Commercialization Aspects of listed Intellectual Property Items

C.1 Patentability of Intellectual Property

Electronic and optical properties of Se and Te studied above are simulated using Quantum Espresso and Berkeley GW package. Since, the work is theoretical there is no patentability.

C.2 Commercialization Prospects

No device was fabricated and there is no aspect of commercializing. This work will aid in experimental and applied studies.

C.3 Possible Prior Disclosure of IP

The electronic properties up to DFT level have already been published. Also, the GW band structure and electronics properties have been studied before, but, it is limited by the vacuum and number of unoccupied bands. The novelty of this work includes an in-depth study of electronic and excitonic properties of Se and Te single helical chains with an optimum vacuum along the xy-plane, laqrge number of conduction bands and optimum number of k-points. The results are published in the paper given below:

“Exfoliation energy, quasiparticle band structure, and excitonic properties of selenium and tellurium atomic chains.” (Phys. Rev. B 98, 035420)

Appendix D: Broader Impact of Research

D.1 Applicability of Research Methods to Other Problems

The simulations carried using Quantum Espresso and Berkeley GW package to perform a GW-BSE calculation can be used to study electronic and excitonic properties for other bulk as well as nano-structured materials. Further, the high value of exciton binding energy obtained in this study can guide the experimental research for fabricating such one-dimensional materials as well as excitonic interconnects and all-optical excitonic transistors.

D.2 Impact of Research Results on U.S. and Global Society

The electronic and optical properties of 1-dimensional materials investigated in this thesis can have a revolutionary effect on the fabrication and manufacturing of opto-electronic devices operating in the Vis-region of the electro-magnetic spectrum, especially for synthesizing mixed dimensional van der Waal's devices and opto-electronic industry. It will aid in experimental R&D work to fabricate and employ such single helical chains of Se and Te.

D.3 Impact of Research Results on the Environment

This work has no inhibitory effects on environment and the materials investigated in this study – Se and Te, also do not exhibit any negative effects on environment. Instead, the experimental fabrication of these devices will have a less toxic effect as compared to conventional GaAs/AlGaAs based Quantum Wells (QWLs).

Appendix E: Microsoft Project for MS MicroEP Degree Plan

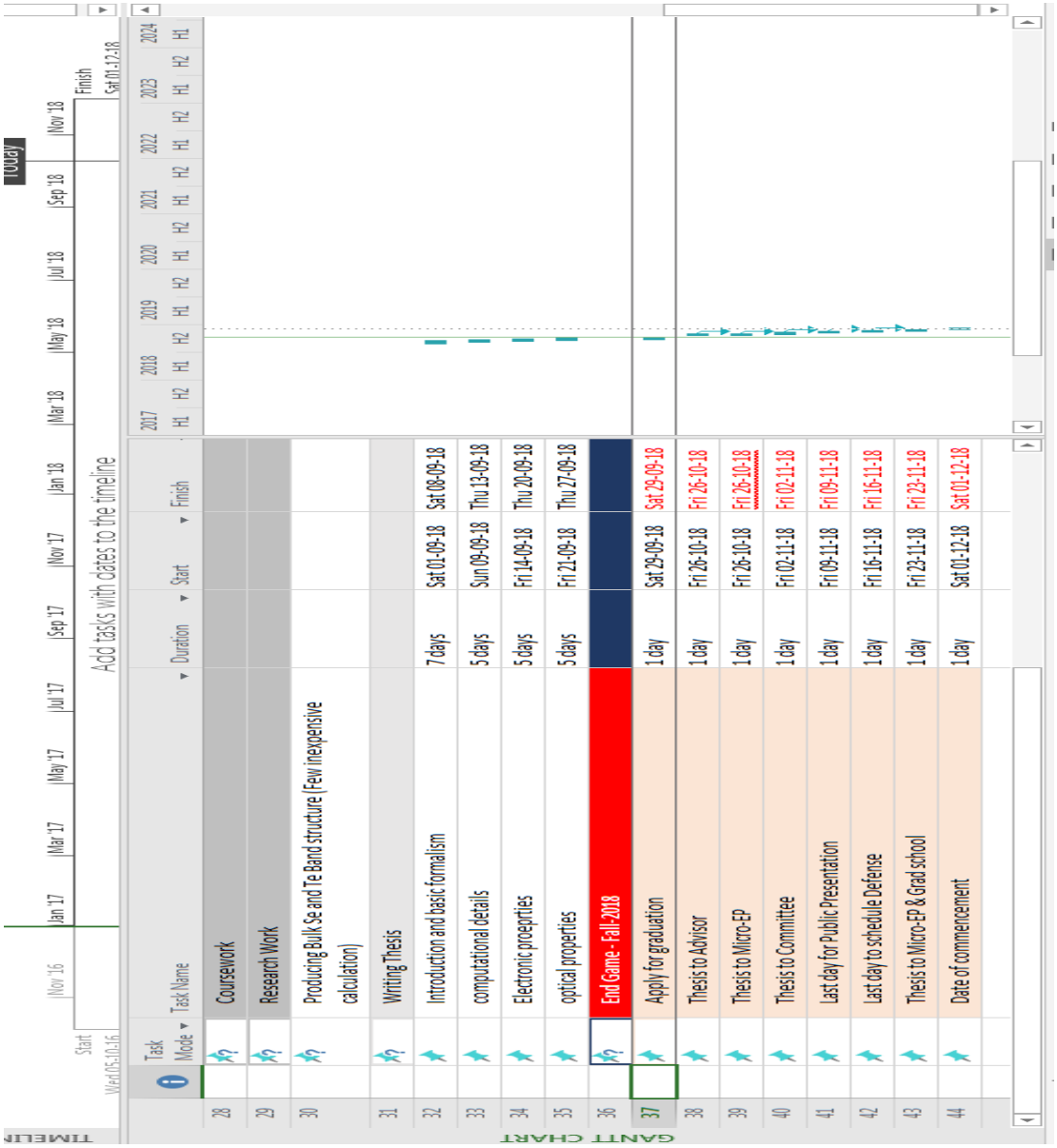

Appendix F: Identification of All Software Used in Research and Thesis Generation

Software #1: MS office 2010
UoA student License
MS EXCEL, MS WORD
Software #2: Xcrysden (visualization of crystal structure)
Freeware software used on Linux OS
Software #3: Xmgrace (for plotting)
Freeware software used on Linux OS
Software #4: Origin Pro version 8.0 (for plotting graphs)
Licensed by Eesha Andharia
Software #5: Quantum Espresso code
Freeware - Version 5.4 by NERSC
Software #6: Berkeley GW code
Freeware - Version 1.2 by NERSC
Software #7: Matlab
UoA student License

Appendix G: All Publications Published, Submitted and Planned

1) “Exfoliation energy, quasiparticle band structure, and excitonic properties of selenium and tellurium atomic chains.”Eesha Andharia, Thaneshwor P. Kaloni, Gregory J. Salamo, Shui-Qing Yu, Hugh O. H. Churchill, and Salvador Barraza-Lopez, Phys. Rev. B 98, 035420 – Published 13 July 2018.